6. TECTONIC IMPLICATIONS OF SMALL EARTHQUAKES IN THE CENTRAL TRANSVERSE RANGES

By JAMES C. PECHMANN[1]

ABSTRACT

Fault-plane solutions for 22 small (local magnitude (M_L)≤4.6) earthquakes in the central Transverse Ranges were determined using an azimuthally varying crustal model. The dominant type of faulting observed is reverse faulting on east-striking planes, which suggests a regional stress field characterized by north-south compression. Some strike-slip faulting also occurs. There is some indication that strike-slip earthquakes may be more common than reverse-slip earthquakes during episodes of crustal dilatation. The rate of north-south crustal shortening attributable to small-earthquake deformation during 1974–76 is two orders of magnitude smaller than the north-south contraction of 0.3 parts per million per year measured at the surface. The scatter in earthquake hypocenters and the general inconsistency of focal mechanisms with geologically determined motions on nearby major faults indicate that the small earthquakes in this region are not associated with large-scale block movements along major fault systems. Rather, they appear to represent fracturing along random minor zones of weakness in response to the regional stress field or, alternatively, small-scale block movements that are below the resolution of this study. Earthquakes in the San Gabriel Mountains north of the Santa Susana-Sierra Madre-Cucamonga frontal fault system tend to concentrate near the eastern and western ends of the range, where good evidence for late Quaternary movement along the frontal faults has been found. Seismicity is markedly lower north of the central section of the frontal fault system, where evidence for late Quaternary movement is lacking.

INTRODUCTION

The Transverse Ranges province of southern California is a complex east-trending geomorphic and structural unit that interrupts the northwest-trending tectonic grain of the Pacific-North American plate boundary (Bailey and Jahns, 1954; Jahns, 1973). In this region the San Andreas fault turns sharply from its general southeast orientation to strike east-southeastward across the Transverse Ranges before splintering into several major branches and continuing southeastward to the Gulf of California (Allen, 1968). South of this San Andreas "big bend" is a broad zone of roughly east-trending, north-dipping thrust and reverse faults including the Santa Monica, Santa Susana, Sierra Madre, and Cucamonga frontal fault systems (fig. 6.1), along which mountain blocks of the central and western Transverse Ranges have been thrust upward and southward.

Interest in the tectonics of the central Transverse Ranges has increased since 1970 because of several developments, notably the following five: (1) The documentation of right-lateral shear-strain accumulation along the locked "big bend" segment of the San Andreas fault (Prescott and Savage, 1976; Savage and others, 1981a, b) contemporaneous with at least partial strain release along the fault system to the northwest and southeast by creep and moderate earthquakes (Allen, 1968, 1982; Harsh and others, 1978; Burford and Harsh, 1980). (2) The occurrence of the 1971 San Fernando earthquake (local magnitude (M_L)=6.4) along the western end of the Sierra Madre fault system (U.S. Geological Survey, 1971; Murphy, 1973; Oakeshott, 1975). (3) The reported formation between 1959 and 1974 of a vertical crustal uplift throughout most of the Transverse Ranges province (Castle and others, 1976). Leveling data indicate that this uplift, the so-called Palmdale bulge, reached a maximum of 35 cm within the study area (fig. 6.1) and then partially subsided between mid-1974 and mid-1976 (Bennet, 1977; Mark and others, 1981). However, serious questions have been raised regarding the accuracy of the leveling data which define the uplift (Jackson and Lee, 1979; Strange, 1981), and the Palmdale bulge is currently a matter of great controversy (Kerr, 1981). (4) The occurrence from 1976 to 1977 of an earthquake swarm along the locked section of the San Andreas fault (fig. 6.1). This swarm was the first observed along this section of the San Andreas since cataloging of instrumental data began in 1932 (McNally and others, 1978). (5) Abrupt changes in the horizontal strain accumulation patterns in southern California that were detected in 1978 and 1979. The measured changes were particularly large on geodetic networks in the Transverse Ranges (Savage and others, 1981a, b).

Vastly improved data on earthquakes in southern California have become available through the increase in the number of stations in the California Institute of Technology/U.S. Geological Survey seismographic network from 39 stations in 1972 to nearly 150 stations in 1978 (Whitcomb, 1978) to over 200 stations in 1983.

[1]Seismological Laboratory, California Institute of Technology, Pasadena, California 91125; present address: Department of Geology and Geophysics, University of Utah, Salt Lake City, Utah 84112.

Manuscript received for publication on June 19, 1979.

Studies of southern California crustal structure using the expanded array (Kanamori and Hadley, 1975; Hadley and Kanamori, 1977; Hadley, 1978) have made possible more accurate interpretations of the earthquake data. Previous studies of earthquakes in the central Transverse Ranges have dealt primarily with the San Fernando earthquake and its aftershocks (Whitcomb and others, 1973; Hadley and Kanamori, 1978) and with microearthquake data from small temporary arrays (Hadley and Combs, 1974; Murdock, 1979; Cramer and Harrington, this volume). The purpose of this report is to present seismicity and focal-mechanism data for the entire central Transverse Ranges area and to discuss their tectonic significance in terms of the geologic evidence concerning long-term deformation and also in terms of the available geodetic evidence pertaining to short-term deformation. The first three sections present a regional study of seismicity and focal mechanisms completed in January 1979. The following section summarizes some results of a later study by Sauber and others (1983), which suggest that changes in

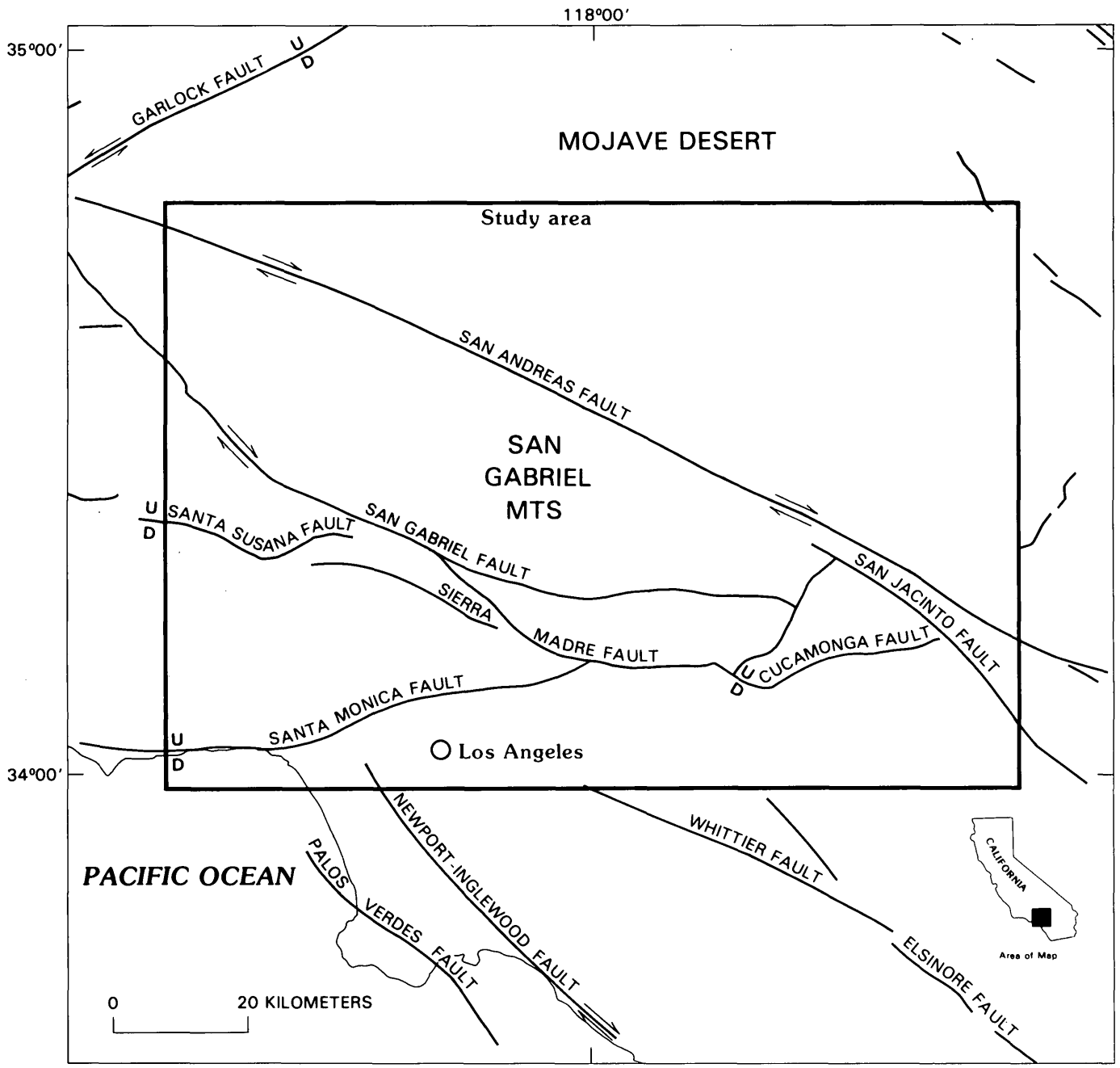

FIGURE 6.1.—Locations and senses of motion of major fault systems within the central Transverse Ranges, generalized from Jennings and others (1975). Arrows show relative horizontal (strike-slip) movement. U and D indicate upthrown and downthrown sides of dip-slip faults.

the regional strain accumulation pattern that took place in late 1978–79 triggered changes in focal mechanisms and in the level of small earthquake activity near Palmdale. These two studies suggest a model for the relationship of small earthquakes in the central Transverse Ranges to strain accumulation on the San Andreas and frontal fault systems that is outlined in the concluding section.

ACKNOWLEDGMENTS

I would like to thank Clarence Allen for suggesting this research and providing encouragement and advice. Dave Hadley, Carl Johnson, and Jim Whitcomb supplied computer programs and many helpful suggestions. Discussions with Karen McNally, Bernard Minster, John Cipar, Hiroo Kanamori, Tracy Johnson, and many others at the California Institute of Technology Seismological Laboratory were also of great benefit. This research was supported in part by the United States Geological Survey, Contract No. 14-08-0001-15258, and by the NASA Office of Applications Grant #NSG5224. This report is Contribution Number 3198, Division of Geological and Planetary Sciences, California Institute of Technology, Pasadena, California 91125.

SEISMICITY, 1933-1977

Epicenter locations are shown in figures 6.2 and 6.3 for all earthquakes located by the California Institute of Technology (Caltech) between 1933 and 1977 within the study area shown in figure 6.1. Faults shown in figure 6.1 are generalized from Jennings and others (1975). Epicenters and magnitudes are taken directly from the Caltech/U.S. Geological Survey southern California earthquake catalog (Hileman and others, 1973; Friedman and others, 1976; Whitcomb and others, 1978). Since location techniques and the density of seismographic stations have changed greatly through the years, these maps must be interpreted with care. Prior to 1961 epicentral determinations were done graphically and reported to the nearest minute. This explains the tendency of epicenters to line up in north-south and east-west directions on the earlier maps. Because the preliminary 1977 catalog was used, hypocentral locations for 1977 are subject to slight modification, quarry blasts have not been removed, and magnitude determinations for the smaller events are incomplete. Quarry locations are indicated by a "Q" in figure 6.3. Earthquakes in 1977 for which magnitudes had not yet been determined are plotted as having $M_L \leqslant 2$ in figure 6.3 but may lie in the range $2 < M_L \leqslant 3$.

Examination of figure 6.3 shows that despite a much-improved detection capability and greater location accuracy, the epicenters still do not show much tendency to cluster near the surface traces of faults. The only exceptions are along the San Jacinto fault and along a northeast-trending feature south of the Cucamonga fault previously identified by Hadley and Combs (1974) on the basis of a microearthquake survey. Hadley and Combs actually found two northeast-trending clusters 5 km apart in this area, the northern one being coincident with the Fontana water barrier. Several aftershock sequences and localized swarms show up very well on the seismicity maps in figures 6.2 and 6.3. The San Fernando aftershock zone is a prominent feature north of the Sierra Madre fault system in the western half of both the 1971–73 and 1974–77 maps. The 1972 Ontario swarm shows up very clearly as a dense cluster near the southeastern corner of the 1971–73 map. The epicenters in figure 6.3 near the western end of the surface trace of the Santa Susana fault are mostly aftershocks from a magnitude 4.6 event on April 8, 1976. This event is noteworthy because of its large number of aftershocks and its unusually great depth of 18 km. The 1976–77 swarm just to the south of the San Andreas fault in the center of figure 6.3 has been studied by McNally and others (1978). The subsequent increase in seismicity here and to the northwest along the San Andreas fault has been shown to be real. However, it is not clear whether the apparent increase in seismicity after 1973 in the Mojave Desert to the northeast of the San Andreas fault (compare figs. 6.2 and 6.3) is real or merely an artifact of improved station coverage.

The scatter in the epicenters of $M_L < 6.0$ shocks in southern California and the general lack of clear spatial relationships between these shocks and recognized faults have often been noted (Richter, 1958; Allen and others, 1965). Important exceptions to the rule are the concentrations of seismicity to the southeast of the study area associated with the Imperial, Brawley, and San Jacinto faults (Friedman and others, 1976; Whitcomb and others, 1978). All of these faults are dominantly strike-slip faults which are known to be creeping (Johnson and Hadley, 1976; Goulty and others, 1978; Keller and others, 1978). Although the San Jacinto fault and its zone of seismicity extends into the southeastern corner of the study area (figs. 6.1 and 6.3), creep has not been demonstrated along this segment of the San Jacinto but only along sections to the southeast. The general scattering of epicenters throughout most of the central Transverse Ranges is perhaps not surprising, given the large number of Quaternary dip-slip faults in the area, most of which are either known or presumed to be of shallow dip (Jennings and others, 1975). Although most recent (post-1974) determinations of epicentral locations are probably accurate to within 2–3 km in this area, comparable accuracy in the hypocentral depth is difficult to obtain. The available data are of sufficient quality to rule out a concentration of hypocenters along a single great megathrust cropping out

along the frontal fault system and dipping northward beneath the mountains. However, careful relocations using a master-event technique may in the future serve to delineate and characterize a series of separate faults, as has been done for the western Transverse Ranges (Lee and others, 1979).

A noteworthy feature of the 1974–77 seismicity map (fig. 6.3) is that in the mountains north of the Santa Susana-Sierra Madre-Cucamonga frontal fault systems most of the seismicity is concentrated to the west and to the east, with comparatively few epicenters located in the central part of the San Gabriel mountains between the eastern Sierra Madre and San Andreas fault zones. This same pattern has been present at least since 1961, when computer location of earthquakes began at Caltech (fig. 6.2). Relocation of selected earthquakes before 1961 using arrival times on file at Caltech has shown that additional work is necessary in order to extend this analysis farther back in time. Available geologic evidence concerning the long-term seismicity correlates well with these observa-

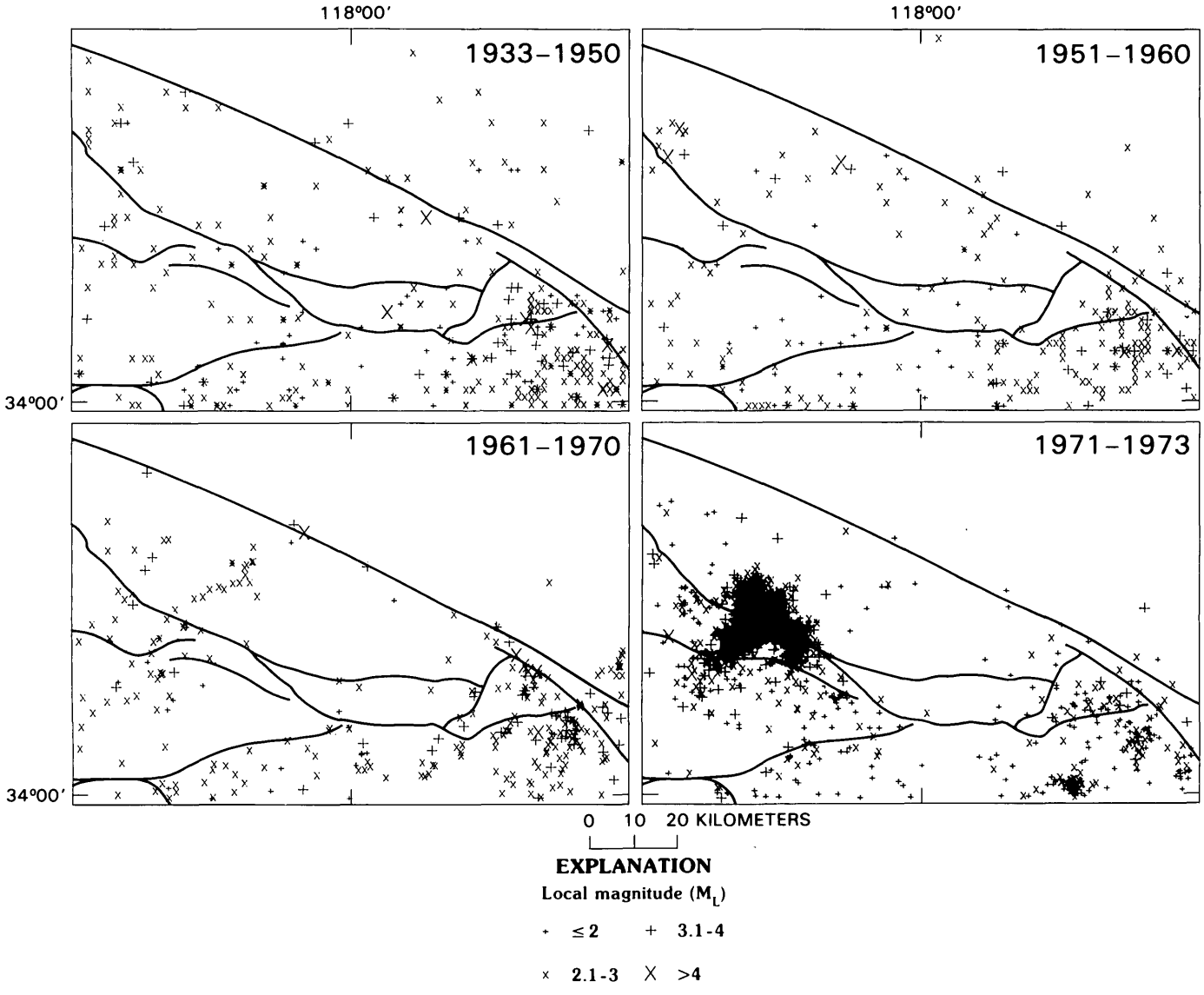

FIGURE 6.2.—Epicenters of all earthquakes located by the California Institute of Technology within the study area for various time intervals. Different symbols indicate local magnitude (M_L) as shown. See figure 6.1 for fault names.

tions. Crook and others (this volume) have found that evidence for late Quaternary movement is lacking in the central part of the San Gabriel frontal fault system south of this gap but is present to the east and to the west. Since geodolite measurements by Savage and others (1978; 1981a, b) indicate that the post-Miocene north-south crustal shortening of the Transverse Ranges (Jahns, 1973) is still occurring, it appears that within the central San Gabriel mountains this deformation must at present be taking place aseismically. This may mean that the deformation here is taking place at a greater depth than elsewhere.

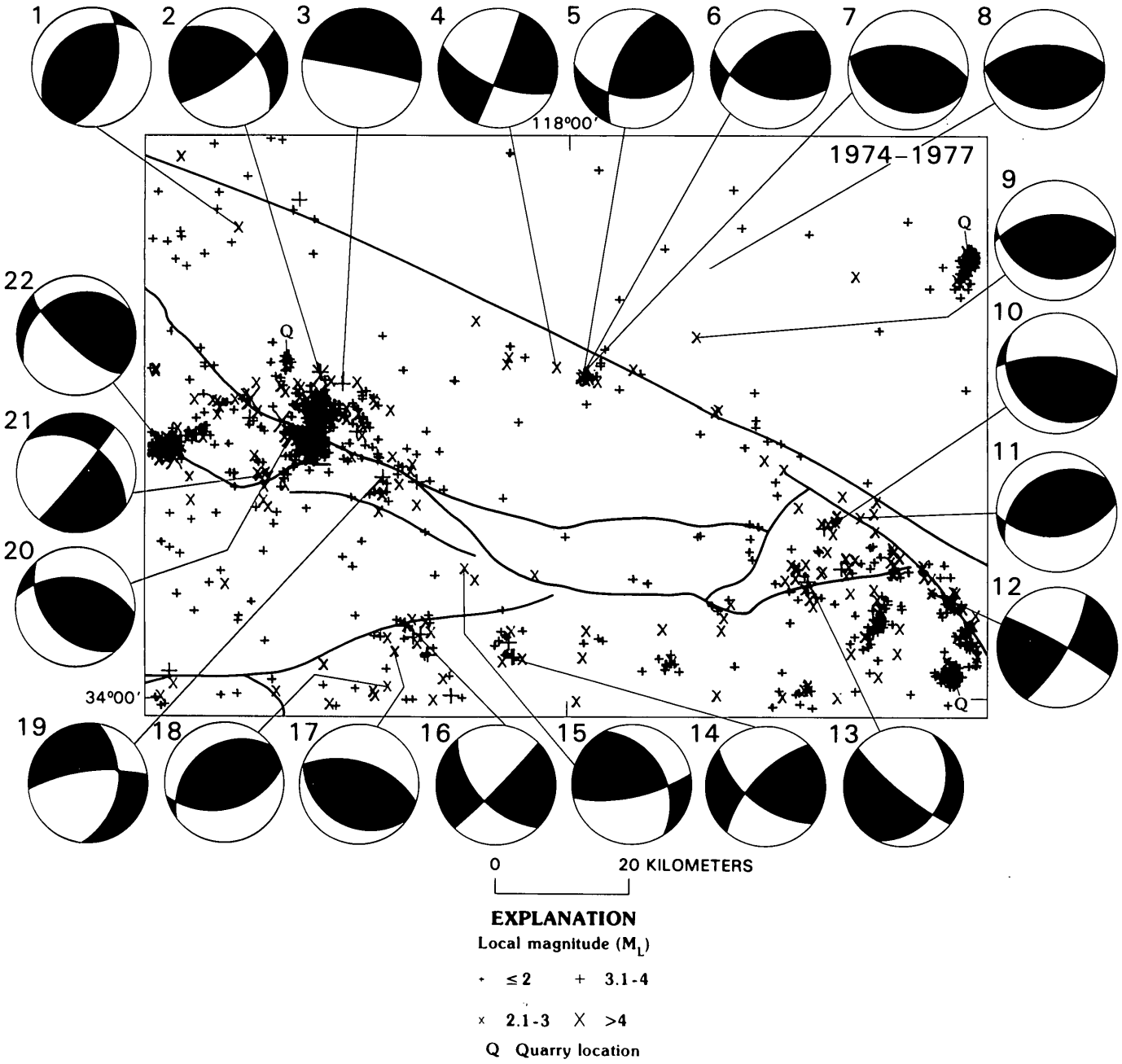

FIGURE 6.3.—Locations of focal mechanisms of figure 6.5 and epicenters of all earthquakes located by the California Institute of Technology within the study area for the time interval 1974–77. Shaded quadrants are compressional. See figure 6.1 for fault names.

TABLE 6.1.—*Events selected for regional focal mechanism study*

[For locations and fault-plane solutions of events, see figs. 6.3 and 6.5, respectively]

Event	Date (mo/d/yr)	Origin time (G.m.t.)	M_L	Caltech catalog location					Revised depth[1] (km)
				Lat (N)		Long (W)		Depth (km)	
1	11/07/76	1421	2.6	34°	40.20'	118°	33.10'	8.0	7.5
2	12/08/76	0213	3.3	34°	28.13'	118°	24.52'	12.4	13.3
3	10/17/76	0538	3.9	34°	27.16'	118°	22.26'	14.9	11.2
4	12/13/76	0826	2.2	34°	28.56'	118°	0.60'	5.9	8.2
5	01/01/77	0100	2.8	34°	27.49'	117°	57.69'	5.4	8.7
6	03/07/77	1104	3.0	34°	27.68'	117°	58.18'	8.0	9.1
7	09/06/77	0508	3.0	34°	27.95'	117°	57.93'	7.2	8.7
8	06/19/78	0741	3.0	34°	37.07'	117°	45.02'	6.7	7.6
9	11/03/76	1741	2.6	34°	31.11'	117°	46.40'	8.0	10.1
10	12/30/76	0225	2.6	34°	15.64'	117°	32.37'	5.0	10.2
11	05/29/76	2038	3.0	34°	15.93'	117°	29.86'	4.7	13.3
12	11/05/75	0237	3.0	34°	9.66'	117°	22.70'	7.2	8.0
13	01/13/75	2328	3.3	34°	10.64'	117°	35.16'	3.6	8.0
14	12/19/74	1236	3.5	34°	4.38'	118°	4.80'	9.2	6.4
15	11/06/74	0038	3.0	34°	11.71'	118°	9.96'	1.0	3.4
16	03/15/77	0801	2.2	34°	6.94'	118°	15.73'	8.8	10.1
17	11/30/76	2355	2.5	34°	4.76'	118°	16.93'	8.0	8.0
18	06/27/76	2211	2.9	34°	1.86'	118°	17.67'	10.4	8.0
19	12/27/75	2108	3.1	34°	19.37'	118°	18.14'	2.1	4.7
20	08/12/77	0219	4.5	34°	22.78'	118°	27.52'	9.5	10.1
21	08/09/76	1054	2.8	34°	19.62'	118°	30.97'	8.0	0.4
22	04/08/76	1521	4.6	34°	20.81'	118°	39.34'	14.5	17.9

[1]The changes in epicentral (horizontal) locations averaged 2.2 km and in all cases were less than 6 km.

FOCAL-MECHANISM DETERMINATIONS

In determining focal mechanisms of local earthquakes from *P*-wave first-motion diagrams, the principal uncertainty is calculating the takeoff angles for first-arrival ray paths. These angles are highly dependent upon the assumed crustal structure and hypocentral depth. For this study a four-layer crustal model based on the work of Hadley and Kanamori (1977) and Hadley (1978) was used. The model consists of a 5-km-thick surface layer (5.5 km/s) underlain successively by upper crust, (6.1–6.3 km/s), lower crust, (6.6–6.8 km/s), and an upper-mantle halfspace (7.8 km/s) beginning at a depth of 33 km (inset, fig. 6.4). The interface between the low-velocity upper crust and the high-velocity lower crust, the Conrad discontinuity, is located at a depth of about 15 km in the central part of the study area. To the northeast in the Mojave Desert this discontinuity is much deeper, only about 5 km above the Mohorovičić discontinuity (Moho), but in the southwest corner of the study area in the Santa Monica Mountains it shallows to a depth of perhaps 10 km. Although in general the Conrad discontinuity appears to dip to the northeast in the central Transverse Ranges, the details of its geometry are poorly known. This creates particular problems in locating earthquakes and determining focal mechanisms, especially since in some areas the discontinuity is located within the seismic zone, which here extends to a depth of about 15 km. One approach to this problem is to employ a model consisting of many horizontal layers, so that the Conrad discontinuity can be smoothed out into a gradient over a depth of 10 km. This technique was used by Hadley and Kanamori (1978). The advantage of this technique is that it reduces the sensitivity of the focal mechanism to changes in the depth of the source. In this study a different, and hopefully more accurate, method is used.

Events for the regional focal-mechanism study were chosen more or less at random, although some attempt was made to obtain a representative geographical distribution within the study area. Twenty-two events ranging in magnitude from 2.2 to 4.6 were selected for study from the time period 1974 to 1978 (table 6.1). To determine the focal mechanisms, arrival times and first motions were first read from 16-mm Develocorder film viewed at a scale of 1 cm/s. These data were supplemented in many cases by readings from Helicorder paper records, films from temporary trailer stations, and computer-stored seismographic traces from the Caltech Earthquake Detection and Recording (CEDAR) system (Johnson, 1979). The 22 earthquakes were then relocated using the computer program HYPO71 (Lee and Lahr, 1975) and a horizontally layered version of the model shown in figure 6.1. Only stations within 60 km of the epicenter were used in order to maximize the depth resolution and minimize the use of arrival times from the dipping Conrad discontinuity, placed at a depth of 15 km in the location model. The average number of stations used for each relocation was 12. Reduced traveltime, $T-\Delta/6.0$, was then plotted

against distance, Δ, for various azimuth ranges. An interpretation of each plot was made in terms of the Hadley-Kanamori model, and then traveltime information was used to assign takeoff angles individually for each station. An example of this method is shown in figure 6.4 for event number 20 (table 6.1), a local magnitude 4.5 event that occurred on August 12, 1977, at a depth of about 10 km. The reduced-traveltime plots for azimuth ranges I and IV clearly show two branches. Arrivals labelled P_g are interpreted as direct waves with an apparent velocity near 6.2 km/s beyond about Δ = 50 km. The branch labelled P_n corresponds to critically refracted waves from the Moho with an apparent velocity of about 7.8 km/s. Refracted waves from the lower crust called P^* are not observed as first arrivals in regions I and IV because the Conrad discontinuity deepens too quickly in these directions. However, to the south of the source in region III, where the Conrad discontinuity shallows, the reduced traveltimes show an apparent velocity close to 6.6 km/s, indicating that all of the arrivals in this azimuth range are probably P^*. The reduced- traveltime plot for azimuth range II, which is roughly along the strike of the Conrad

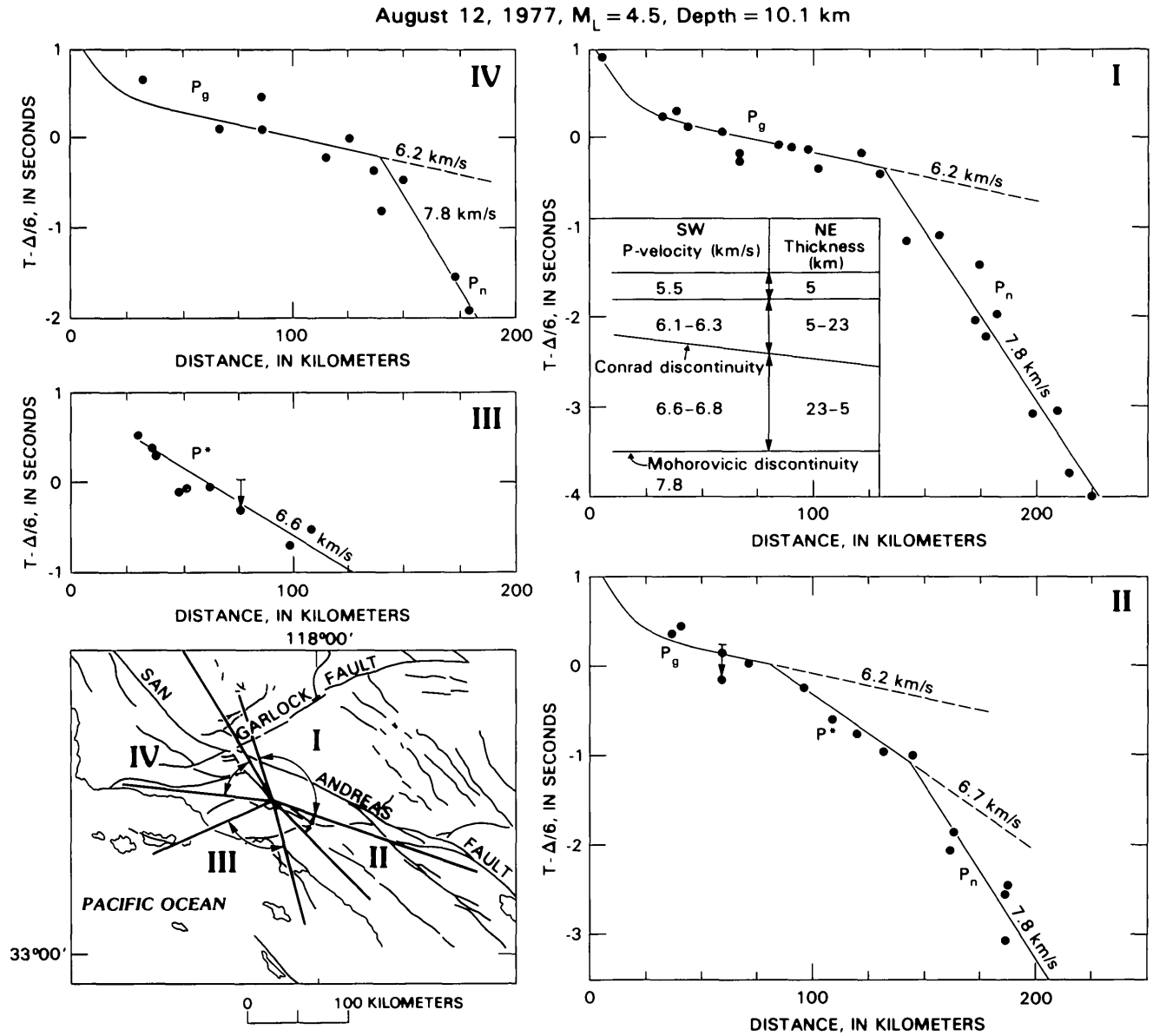

FIGURE 6.4.—Plots of reduced traveltime, T – Δ/6, versus distance, Δ, for event number 20 (table 6.1) for the four azimuth ranges shown in the map at lower left. Vertical arrows above some points show deep-sediment corrections determined by Raikes (1978). P_g, P^*, and P_n identify different seismic arrivals discussed in the text. Inset shows the velocity model used to interpret the plots (Hadley and Kanamori, 1977; Hadley, 1978). Dip on the Conrad discontinuity is exaggerated.

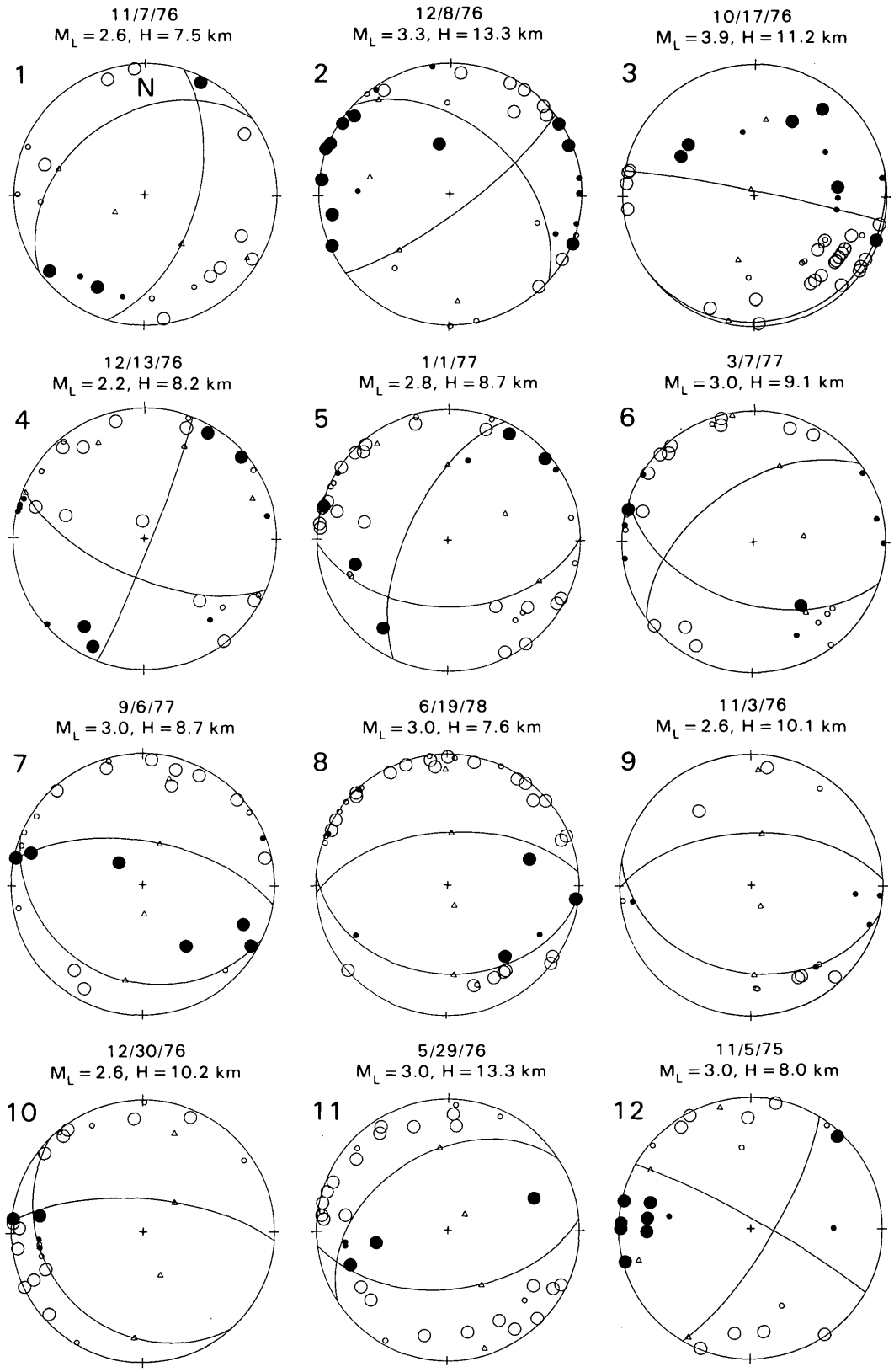

FIGURE 6.5.—Lower hemisphere *P*-wave fault-plane solutions for 22 events in the central Transverse Ranges. Dots indicate compressional first motions; circles indicate dilatational first motions. Good-quality readings of first motions shown by large symbols; fair-quality readings by small symbols. Slip vectors, compression axes, and tension axes are shown with triangles. The date, local magnitude (M_L) and depth (H) are given for each event. Event numbers correspond to those in figure 6.3.

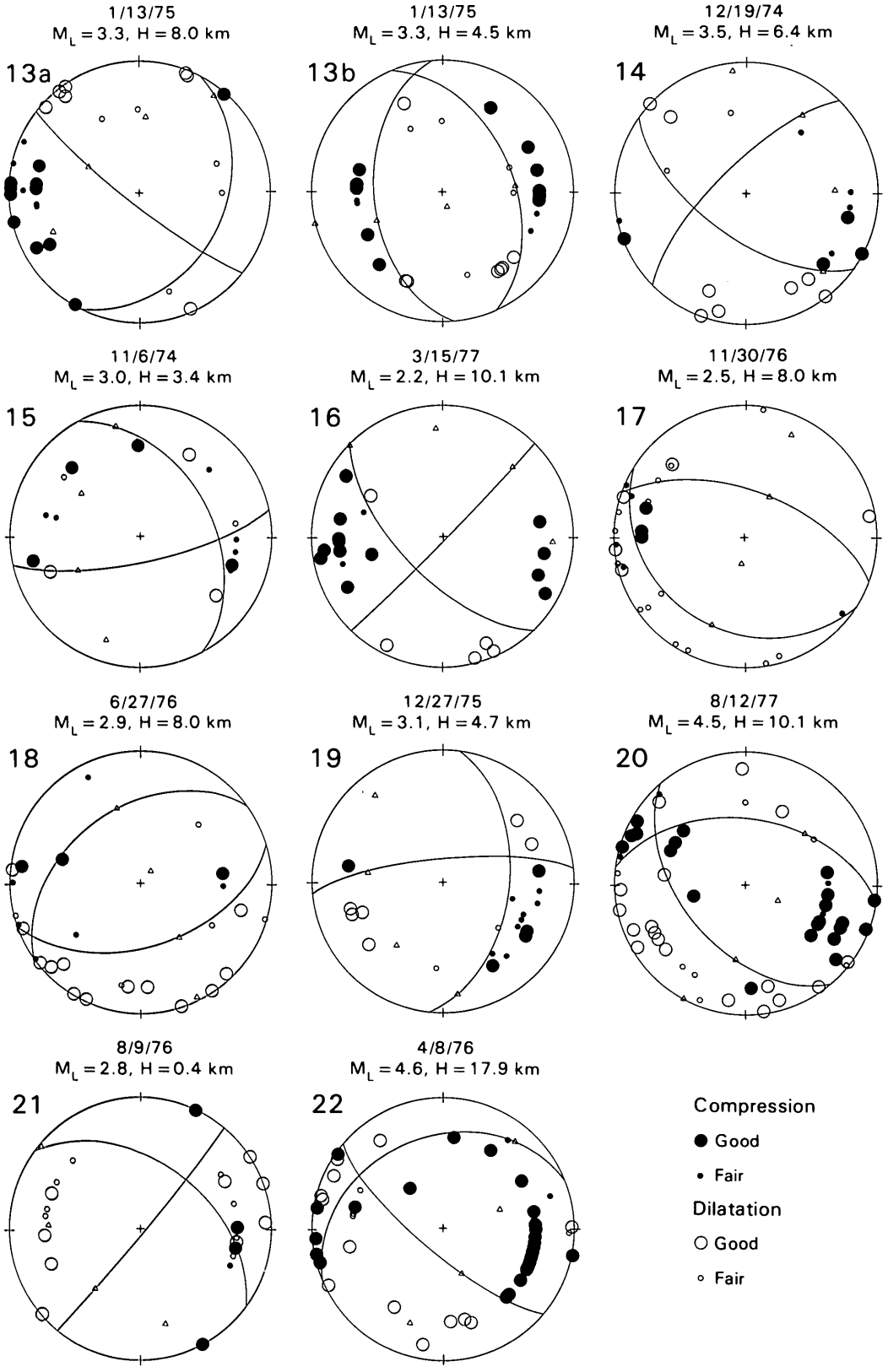

FIGURE 6.5.—Continued.

discontinuity, shows three branches corresponding to P_g, P^*, and P_n. Since the dip on the Conrad discontinuity is not well known but is probably small, the takeoff angles for all three branches of the traveltime curves were calculated using the horizontally layered location model. The resultant P-wave first-motion plot is shown in figure 6.5 (focal mechanism 20).

Use of the technique just described eliminates much of the uncertainty in determining takeoff angles when the source depth is not well constrained. A problem still remains, however, if the event is located near a discontinuity in the velocity model, because the traveltime curves for a source located just above a discontinuity are nearly identical to those for a source located just below it, but the takeoff angles are quite different. When this problem was encountered, the mechanisms were determined for sources located on both sides of the discontinuity, and the mechanism with the fewest stations in error was chosen. Only in one instance were the two mechanisms significantly different and of equal quality, and for this event (focal mechanism 13, fig. 6.5) both solutions are shown.

RESULTS OF REGIONAL FOCAL-MECHANISM STUDY

Figure 6.5 shows the P-wave first-motion plots for the events studied. The nodal planes were determined with the aid of the computer program FOCPLT developed by Whitcomb and Garmany (Whitcomb, 1973). This program tests a grid of trial mechanisms spaced at approximately 5-degree intervals on the focal sphere and then chooses a mechanism which minimizes the number of first-motion readings in error. Less reliable readings are given half the weight of other readings, and a linear function is used to downweight stations within 3 degrees of a nodal plane. Most of the focal mechanisms shown in figure 6.5 are well-constrained. The numbers are keyed to figure 6.3, which shows the location of each mechanism.

Examination of figure 6.3 shows that there is little systematic variation in mechanism from place to place within the study area. Most of the solutions show strike-slip faulting, reverse faulting, or a combination of strike-slip and reverse faulting. In general, the fault-plane orientations and senses of motion do not agree very well with those of the major faults shown. Along the San Jacinto fault, mechanism 12 is consistent with geologic evidence for right-lateral strike-slip motion on a northwest-trending fault. However, 20 km to the northwest along the same fault zone, thrusting is observed. Mechanisms 4, 5, 6, and 7 are especially interesting because master-event relocations for these events by McNally and others (1978) show that they all cluster within a small volume 3 km in maximum dimension, centered 2 km southwest of the mapped surface trace of the San Andreas fault at a depth of about 8 km. Although mechanism 4 is consistent with the long-term sense of motion on the San Andreas fault, the others are not and, furthermore, show systematic changes in mechanism with time. This swarm may be associated with the San Andreas fault or with one of several subparallel faults that splay southward from the main fault at this point. Focal mechanisms for events 3, 20, and 22 agree well with those determined independently by Hadley and Kanamori (1978). Two of these, events 3 and 22, are consistent with motion on either nearly vertical or nearly horizontal planes. Hadley and Kanamori argue on the basis of these mechanisms and other evidence that regional horizontal decollements may exist within the central Transverse Ranges. If the horizontal plane in mechanisms 3 and 22 is chosen as the fault plane, then movement of the upper block is towards the south or southwest.

Although the fault-plane solutions in figure 6.5 show considerable diversity, the compression axes for most of them are oriented nearly north-south and horizontal. Other investigators have obtained similar results in the central Transverse Ranges (Whitcomb and others, 1973; Cramer and Harrington, this volume). In the western Transverse Ranges the compression axis is still the most stable parameter, but the preferred orientation is closer to north-northeast—south-southwest and horizontal (Stierman and Ellsworth, 1976; Corbett and Johnson, 1982; Yerkes and Lee, this volume). Earthquakes in the eastern Transverse Ranges have focal mechanisms characterized by north-south compression axes and east-west tension axes (Webb and Kanamori, 1985).

To produce a combined plot of the compression axes that reflected the degree of constraint of the mechanisms, I used the grid of scores calculated by FOCPLT for each event. Positions of the compression axes corresponding to best-fit solutions with the minimum numbers of stations in error were assigned a weight of 3. Positions that allowed less than one additional good-quality reading or two additional fair-quality readings to be in error were assigned a weight of 2. Positions with the number of stations in error beyond the minimum lying in the range 1–2 good or 2–4 fair were given a weight of 1. Scores worse than this were given zero weight. The weights for all the events were added up at each focal-sphere grid point and the results contoured to give the plot shown in figure 6.6. A similar diagram for the tension axes is also shown.

Figure 6.6 clearly demonstrates that focal mechanisms in the central Transverse Ranges are characterized by a horizontal north-south compression axis and a nearly vertical tension axis. The dominant type of faulting is, therefore, reverse faulting on east-striking planes with dip near 45°. Even though compression and tension axes for individual earthquakes do not necessarily reflect the actual tectonic stress field (McKenzie, 1969), the well-defined maxima in figure 6.6 suggest that these parameters have

physical significance in a statistical sense. The north-south compression suggested by the fault-plane solutions is consistent with the north-northwest orientations for maximum horizontal compressive stress measured in boreholes in this region (Flaccus and others, 1980; Zoback and others, 1980). There is, in addition, abundant geologic evidence to suggest strong north-south compression in the Transverse Ranges province during post-Miocene times. This north-south compression has resulted in folding along east-west axes, thrust and reverse faulting with some components of strike-slip, and major uplift of several crustal blocks (Jahns, 1973).

A more direct conclusion that can be drawn from figure 6.6 is that the average deformation resulting from small earthquakes in this region is north-south crustal shortening and vertical extension, at least for the time period 1974 to 1978. Since this is permanent deformation, it constitutes a form of elastic strain relief. Geodolite measurements of horizontal strain accumulation by Savage and others (1978) in the interval from 1972 to 1978 indicate a remarkably consistent uniaxial north-south contraction of about 0.2–0.3 parts per million per year (ppm/yr) throughout southern California. This strain apparently accumulated uniformly with time. The amount of north-south contraction attributable to faulting during small earthquakes is therefore relevant to the rate of stress accumulation across both the San Andreas and frontal fault systems.

Kostrov (1974) derives an expression to describe how movements in separate earthquakes along numerous randomly located fractures can be summed in a quasi-plastic deformation process. The expression is

$$\dot{\varepsilon}_{ij} = \frac{1}{2\mu\Delta v\Delta t} \sum_{\varkappa} M_{0ij}^{(\varkappa)},$$

where $\dot{\varepsilon}_{ij}$ is the mean tensor of the rate of deformation due to the seismic flow of rock masses, Δv and Δt are the volume and time interval, respectively, over which the $M_{0ij}^{(\varkappa)}$ are summed, μ is the rigidity, and $M_{0ij}^{(\varkappa)}$ is the ij'th component of the moment tensor of the $\varkappa$th earthquake. If M_0 is the moment,

$$M_{0ij} = M_0 (b_j n_i + b_i n_j),$$

where $\vec{b}$ is a unit vector in the displacement direction and $\vec{n}$ is a unit vector perpendicular to the fault plane. To estimate the mean tensor of the rate of seismic deformation in the central Transverse Ranges, we assume that the average $\vec{b}$ and $\vec{n}$ vectors are those corresponding to the average mechanism indicated by figure 6.6. In a coordinate system with the X_1-axis directed eastward, the

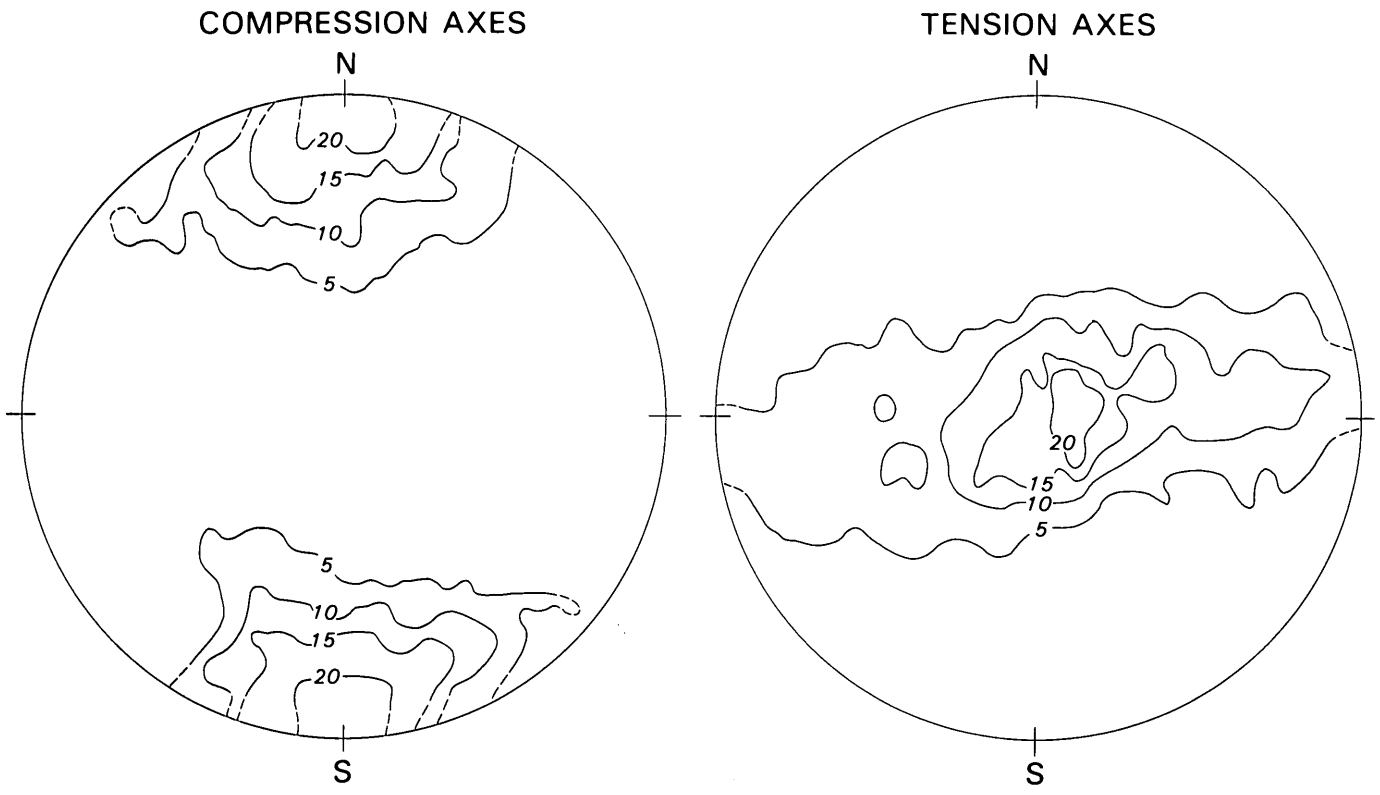

FIGURE 6.6.—Orientation of compression and tension axes on the focal sphere, taking into account variation of quality of mechanisms in figure 6.5. See text for explanation.

X_2-axis northward, and the X_3-axis upward, the expression for $\dot{\varepsilon}_{ij}$ reduces to

$$\dot{\varepsilon}_{33} = -\dot{\varepsilon}_{22} = \frac{1}{2\mu\Delta v\Delta t}\sum_{\kappa} M_0^{(\kappa)}$$

with all other components zero. Since the mechanisms were determined for earthquakes during the time period 1974–1978, but post-1976 magnitudes were incomplete, we calculated $\dot{\varepsilon}_{33}$ for the three-year period 1974–1976. Define $n(M)$ to be the number of events with local magnitude greater than or equal to M during this period within the boxed area of figure 6.1. Since all earthquakes that occurred during this time were less than magnitude 5.0, and earthquakes of magnitude less than 0.0 have negligibly small moments, we can write

$$\dot{\varepsilon}_{33} \approx \frac{-1}{6\mu\Delta v}\int_0^{5.0} M_0(M)\,\frac{dn(M)}{dM}\,dM$$

where $M_0(M)$ is an empirical moment-magnitude relationship. On the basis of Wyss and Brune (1968), Thatcher and Hanks (1973), Bakun (1984), and Hanks and Boore (1984), we use the following relationship for $M_0(M)$

$$\log M_0 = 1.5M + 16.0 \qquad 3.3 \leqslant M \leqslant 5.0$$

$$\log M_0 = 1.2M + 17.0 \qquad 0.0 \leqslant M \leqslant 3.3$$

The function $n(M)$ was found to be given to a good approximation by

$$\log n = 4.5 - 1.0M.$$

Since most earthquakes in the study area occur at depths less than 15 km, we set the volume Δv equal to the area of the box in figure 6.1 times 15 km. This gives $\Delta v = 1.7 \times 10^{20}$ cm^3. Assuming $\mu = 2 \times 10^{11}$ dynes/cm^2 and substituting into the above expression, the result is $\dot{\varepsilon}_{33} = -\dot{\varepsilon}_{22} \approx 1 \times 10^{-9}$/year.

This number is two orders of magnitude smaller than the rate of north-south contraction determined geodetically at the surface for the same time period. We conclude that seismic faulting during 1974–76 within the study area can account for only a negligibly small amount of the measured north-south contraction. Hence, most of the contraction must represent either elastic strain accumulation or aseismic deformation.

EVIDENCE FOR TEMPORAL CHANGES IN FOCAL MECHANISMS

Shortly after this regional focal-mechanism and seismicity study presented above was completed in January 1979, changes were detected in the horizontal strain accumulation patterns in southern California through two different geodetic monitoring techniques: interferometry measurements using extraterrestrial radio sources (P. F. MacDoran, unpub. data from the Aries Project, 1980) and ground-based trilateration with a laser-ranging device (Savage and others, 1981a, b). The horizontal-strain accumulation across all three of the U.S. Geological Survey trilateration networks that lie within or partially within the central Transverse Ranges was a uniaxial north-south contraction of 0.2–0.3 ppm/yr from 1971–74, when measurements began, through 1978 (Savage and others, 1978). Between late 1978 and 1979, an episode of both north-south and east-west extension was observed over a region that encompassed at least the northwestern part of the study area. The largest amount of dilatation observed, about 2 ppm, was on the Palmdale trilateration network, which spans a 20-km-long section of the San Andreas fault within the study area (Savage and others, 1981a, b).

The remarkable agreement between the principal strain directions determined from trilateration measurements at the surface and the principal axes of the deformation tensor inferred from small-earthquake mechanisms during the period 1974–78 (fig. 6.6) suggests that small-earthquake mechanisms may accurately reflect the regional strain field even though their contribution to the regional deformation is quite minor. A question therefore arises as to whether or not the 1978–79 strain anomalies were accompanied by changes in the dominant faulting mechanism. In order to search for such changes, a systematic study of focal mechanisms of earthquakes during 1976–80 in the "big bend" region of the San Andreas fault was undertaken by several workers including the author (Sauber and others, 1983). The results of this study are summarized briefly below.

The 26 focal mechanisms (including 7 from this study) analyzed by Sauber and others (1983) generally showed reverse faulting, strike-slip faulting, or a combination of the two and were consistent with north-south compression. Reverse faulting on northeast- to southeast-striking planes was the most common faulting mechanism observed, as was found also for the regional study reported here (figs. 6.5 and 6.6). Around the time of the crustal dilatation episode, however, there appeared to be an unusually large number of strike-slip events. This observation suggests that a change in focal mechanism accompanied the strain changes, but the correlation must be considered tentative because of the limitations of the data (see Sauber and others, 1983).

The change in mechanism from reverse to predominantly strike slip observed by Sauber and others (1983) during the period from mid-1978 to mid-1979 is at least qualitatively consistent with the measured horizontal strain changes and may reflect a change in the tectonic stress field. Within the study area, the most compressive principal stress is roughly north-south. Anderson's (1951) theory of faulting predicts reverse faulting for this region if the least principal stress is vertical and strike-slip faulting if the least principal stress is east-west. Therefore, the change in mechanism from reverse to strike-slip suggests that the least principal stress rotated from near vertical to approximately horizontal and east-west. The east-west extension that began in 1978–79 could have caused such a rotation, depending on the pre-existing stress and the magnitude and sign of any changes in the vertical stress component. Although north-south extension was also observed at this time, it was smaller in magnitude than the north-south compressive strain accumulated over the previous 7 years, and hence the orientation of the most compressive principal stress probably remained approximately north-south.

The maximum linear strain change observed on the Palmdale network was 1.5 ppm. Assuming a linear relation between stress and strain and an elastic modulus of 3×10^{11} dynes/cm^2, this strain change corresponds to a stress change of only half a bar. Thus, changes in the dominant type of faulting mechanism might occur as a result of small changes in stress.

CONCLUSIONS

The overall seismicity within the central Transverse Ranges can best be described as diffuse. Focal mechanisms for recent small earthquakes in this region similarly indicate that most of the seismicity is not directly related to the major Quaternary faults (fig. 6.3). The dominant mechanism of faulting at present appears to be reverse faulting on east-striking planes. Less commonly, strike-slip faulting on generally northwest- or northeast-striking planes is observed. Most mechanisms represent a combination of these two principal fault types, which correspond to the major categories of active fault systems found in this region.

Horizontal-strain accumulation across geodetic networks in the central Transverse Ranges appears to consist of 0.2–0.3 ppm/year of approximately north-south compression, occasionally interrupted by episodes of both north-south and east-west extension. The average deformation resulting from small earthquakes in this region is very similar to the pattern of strain accumulation inferred from surface measurements: north-south crustal shortening, vertical extension, and a lesser amount of east-west extension. However, calculations show that the small earthquakes ($M \leqslant 5$) are relieving only a negligible amount of the accumulating strain. There is some evidence to suggest that strike-slip earthquakes are more common than reverse-slip earthquakes during periods of dilatation. If this is true, faulting in small earthquakes may be sensitive to small changes in the applied stress.

The above observations suggest that a reasonable physical model for the deformation between large earthquakes in this region is quasi-homogeneous north-south crustal shortening accompanied by vertical and east-west extension, which involves elastic-strain accumulation and brittle seismic fracturing near the surface together with viscous or viscoelastic flow at depth. Most of the small earthquakes appear to be part of this quasi-homogeneous deformation process and are not associated with large-scale block movements along major faults. Detailed studies may in some cases serve to identify small earthquakes with small-scale block movements. However, it seems likely that a wide variety of pre-existing zones of weakness exist throughout the region and that slip occurs on those most favorably oriented to the local stress field.

The central Transverse Ranges stress field inferred from fault-plane solutions and near-surface measurements appears to be dominated by north-south compression with the least principle stress axis near vertical. However, the origin of this stress field is not well understood. Simple dislocation models of the San Andreas fault system predict north-northwest to north-northeast compression in the central Transverse Ranges, with an equal amount of horizontally directed tension perpendicular to the compression (Rodgers and Chinnery, 1973; Prescott and Savage, 1976). Bird and Piper (1980) have developed a plane-stress finite-element nonlinear tectonic flow model for southern California that includes a weakened zone along the San Andreas fault. This model comes closer to reproducing the observed stress field, but fails in other respects. Even more puzzling than the origin of the stress field is the cause of the fluctuations in the isotropic strain that occur despite the nearly uniform shear-strain accumulation. Inasmuch as earthquakes are the only source of information about stress conditions deep within the earth, their continued study should prove useful in investigating the above problems.

REFERENCES CITED

Allen, C. R., 1968, The tectonic environments of seismically active and inactive areas along the San Andreas fault system, *in* Dickinson, W. R., and Grantz, Arthur, eds., Proceedings of the conference on geologic problems of the San Andreas fault system: Stanford University Publications in Geological Sciences, v. 11, p. 70–82.

—— 1982, Creep and strain studies in southern California, *in* Summaries of technical reports, National Earthquake Hazards Reduction Program: U.S. Geological Survey Open-File Report 82–65, v. 13, p. 225–227.

Allen, C. R., St. Amand, Pierre, Richter, C. F., and Nordquist, J. M., 1965, Relationship between seismicity and geologic structure in the southern California region: Seismological Society of America Bulletin, v. 55, p. 753–797.

Anderson, E. M., 1951, The dynamics of faulting: Edinburgh, Oliver and Boyd, 206 p.

Bailey, T. L., and Jahns, R. H., 1954, Geology of the Transverse Range province, southern California, *in* Jahns, R. H., ed., Geology of southern California: California Division of Mines Bulletin 170, p. 83–106.

Bakun, W. H., 1984, Seismic moments, local magnitudes, and coda-duration magnitudes for earthquakes in central California: Seismological Society of America Bulletin, v. 74, p. 439–458.

Bennet, Jack, 1977, Palmdale "bulge" update: California Geology, v. 30, p. 187–188.

Bird, Peter, and Piper, K., 1980, Plane-stress finite-element models of tectonic flow in southern California: Physics of the Earth and Planetary Interiors, v. 21, p. 158–175.

Burford, R. O., and Harsh, P. W., 1980, Slip along the San Andreas fault in central California from alinement array surveys: Seismological Society of America Bulletin, v. 70, p. 1233–1261.

Castle, R. O., Church, J. P., and Elliott, M. R., 1976, Aseismic uplift in southern California: Science, v. 192, p. 251–253.

Corbett, E. J., and Johnson, C. E., 1982, The Santa Barbara, California, earthquake of 13 August 1978: Seismological Society of America Bulletin, v. 72, p. 2201–2226.

Flaccus, C. E., Richardson, R. M., Sbar, M. L., Engelder, T., and Yale, D., 1980, Tectonic stress near the San Andreas fault from strain relief measurements [abs.]: Eos (American Geophysical Union Transactions), v. 61, p. 1118.

Friedman, M. E., Whitcomb, J. H., Allen, C. R., and Hileman, J. A., 1976, Seismicity of the southern California region, 1 January 1972 to 31 December, 1974: California Institute of Technology, Division of Geological and Planetary Sciences, Contribution 2734.

Goulty, N. R., Burford, R. O., Allen, C. R., Gilman, Ralph, Johnson, C. E., and Keller, R. P., 1978, Large creep events on the Imperial fault, California: Seismological Society of America Bulletin, v. 68, p. 517–521.

Hadley, D. M., 1978, Geophysical investigations of the structure and tectonics of southern California: Pasadena, California Institute of Technology, Ph.D. dissertation, 167 p.

Hadley, David, and Combs, J., 1974, Microearthquake distribution and mechanisms of faulting in the Fontana-San Bernardino area of southern California: Seismological Society of America Bulletin, v. 64, no. 5, p. 1477–1499.

Hadley, David, and Kanamori, Hiroo, 1977, Seismic structure of the Transverse Ranges, California: Geological Society of America Bulletin, v. 88, p. 1469–1478.

_____ 1978, Recent seismicity in the San Fernando region and tectonics in the west-central Transverse Ranges, California: Seismological Society of America Bulletin, v. 68, no. 5, p. 1449–1457.

Hanks, T. C., and Boore, D. M., 1984, Moment-magnitude relations in theory and practice: Journal of Geophysical Research, v. 89, p. 6229–6235.

Harsh, P. W., Burford, R. O., and Kinugasa, Y., 1978, Rates of fault slip during historic time in central California [abs.]: Eos (American Geophysical Union Transactions), v. 59, p. 1209–1210.

Hileman, J. A., Allen, C. R., and Nordquist, J. M., 1973, Seismicity of the southern California region, 1 January 1932 to 31 December 1972: California Institute of Technology, Division of Geological and Planetary Sciences, Contribution no. 2385.

Jackson, D. D. and Lee, W. B., 1979, The Palmdale bulge—An alternate interpretation [abs.]: Eos (American Geophysical Union Transactions), v. 60, p. 810.

Jahns, R. H., 1973, Tectonic evolution of the Transverse Ranges province as related to the San Andreas fault system, *in* Kovach, R. L., and Nur, Amos, eds., Proceedings of the conference on tectonic problems of the San Andreas fault system: Stanford University Publications in Geological Sciences, v. 13, p. 149–170.

Jennings, C. W., Strand, R. G., Rogers, T. H., Stinson, M. G., Burnett, J. L., Kahle, J. E., Streitz, R., and Switzer, R. A., 1975, Fault map of California with locations of volcanoes, thermal springs and thermal wells: California Division of Mines and Geology, California Geologic Data Map 1, scale 1:750,000.

Johnson, C. E., 1979, I, CEDAR—an approach to the computer automation of short-period local seismic networks, II, Seismotectonics of the Imperial Valley of southern California: Pasadena, California Institute of Technology, Ph.D. dissertation, 343 p.

Johnson, C. E., and Hadley, D. M., 1976, Tectonic implications of the Brawley earthquake swarm, Imperial Valley, California, January 1975: Seismological Society of America Bulletin, v. 66, p. 1133–1144.

Kanamori, Hiroo, and Hadley, David, 1975, Crustal structure and temporal velocity change in southern California: Pure and Applied Geophysics, v. 113, p. 257–280.

Keller, R. P., Allen, C. R., Gilman, Ralph, Goulty, N. R., and Hileman, J. A., 1978, Monitoring slip along major faults in southern California: Seismological Society of America Bulletin, v. 68, p. 1187–1190.

Kerr, R. A., 1981, Palmdale Bulge doubts now taken seriously: Science, v. 214, p. 1331–1333.

Kostrov, V. V., 1974, Seismic moment and energy of earthquakes and seismic flow of rock (Translated by F. Goodspeed): Izvestija, Earth Physics, no. 1, p. 23–40.

Lee, W. H. K., and Lahr, J. C., 1975, HYP071 (revised): A computer program for determining hypocenter, magnitude, and first motion pattern of local earthquakes: U.S. Geologic Survey Open-File Report 75–311, 114 p.

Lee, W. H. K., Yerkes, R. F., and Simirenko, M., 1979, Recent earthquake activity and focal mechanisms in the western Transverse Ranges, California: U.S. Geological Survey Circular 799A, p. A1–A26.

Mark, R. K., Tinsley, J. C., Newman, E. B., Gilmore, T. D., and Castle, R. O., 1981. An assessment of the geodetic measurements that define the southern California uplift: Journal of Geophysical Research, v. 86, p. 2783–2808.

McKenzie, D. P., 1969, The relation between fault plane solutions for earthquakes and the directions of the principal stresses: Seismological Study of America Bulletin, v. 59, p. 591–601.

McNally, K. C., Kanamori, Hiroo, Pechmann, J. C., and Fuis, Gary, 1978, Earthquake swarm along the San Andreas fault near Palmdale, southern California, 1976 to 1977: Science, v. 201, p. 814–817.

Murdock, J. N., 1979, A tectonic interpretation of earthquake focal mechanisms and hypocenters in Ridge Basin, southern California: Seismological Society of America Bulletin, v. 69, p. 417–425.

Murphy, L. M., ed., 1973, San Fernando, California, earthquake of February 9, 1971: U.S. Department of Commerce, National Oceanic and Atmospheric Administration, v. 3, 432 p.

Oakeshott, G. B., ed., 1975,, San Fernando, California, earthquake of 9 February, 1971: California Division of Mines and Geology Bulletin 196, 463 p.

Prescott, W. H., and Savage, J. C., 1976, Strain accumulation on the San Andreas fault near Palmdale, California: Journal of Geophysical Research, v. 81, p. 4901–4908.

Raikes, S. A., 1978, Regional variations in upper mantle compressional velocities beneath southern California: Pasadena, California Institute of Technology, Ph.D. dissertation (part I), 209 p.

Richter, C. F., 1958, Elementary seismology: San Francisco, W. H. Freeman and Co., 768 p.

Rodgers, D. A., and Chinnery, M. A., 1973, Stress accumulation in the Transverse Ranges, southern California *in* Kovach, R. L., and Nur, Amos, eds., Proceedings of the conference on tectonic problems of

the San Andreas fault system; Stanford University Publications in Geological Sciences, v. 13, p. 70–79.

Sauber, Jeanne, McNally, Karen, Pechmann, J. C., and Kanamori, Hiroo, 1983, Seismicity near Palmdale, California, and its relation to strain changes: Journal of Geophysical Research, v. 88, p. 2213–-2219.

Savage, J. C., Prescott, W. H., Lisowski, M., and King, N. E., 1978, Strain in southern California: measured uniaxial north-south regional contraction: Science, v. 202, p. 883–885.

——— 1981a, Strain accumulation on the San Andreas fault near Palmdale, California: Rapid, aseismic change: Science, v. 211, p. 56–58.

——— 1981b, Strain accumulation in southern California, 1973-1980: Journal of Geophysical Research, v. 86, p. 6991–7002.

Stierman, D. J., and Ellsworth, W. L., 1976, Aftershocks of the February 21, 1973, Point Mugu, California, earthquake: Seismological Society of America Bulletin, v. 66, p. 1931–1952.

Strange, W. E., 1981, The impact of refraction correction on leveling interpretations in southern California: Journal of Geophysical Research, v. 86, p. 2809–2824.

Thatcher, Wayne, and Hanks, T. C., 1973, Source parameters of southern California earthquakes: Journal of Geophysical Research, v. 78, no. 35, p. 8547–8576.

U.S. Geological Survey, 1971, The San Fernando, California, earthquake of February 9, 1971: U.S. Geological Survey Professional Paper 733, 254 p.

Webb, T. H., and Kanamori, Hiroo, 1985, Earthquake focal mechnisms in the eastern Transverse Ranges and San Emigdio Mountains, southern California, and evidence for a regional decollement: Seismological Society of America Bulletin, v. 75, no. 3, p. 737–757.

Whitcomb, J. H., 1973, The 1971 San Fernando earthquake series focal mechanisms and tectonics: Pasadena, California Institute of Technology, Ph.D. dissertation (part II).

——— 1978, P and S-phase data from local earthquakes in southern California for 1966 to 1975: Seismological Society of America Bulletin, v. 68, p. 523–525.

Whitcomb, J. H., Allen, C. R., Blanchard, A. C., Fisher, S. A., Fuis, G. S., Hutton, L. K., Jenkins, D. J., Johnson, C. E., Reed, B. A., and Richter, K. J., 1978, Southern California array for research on local earthquakes and teleseisms (SCARLET), Caltech-USGS monthly preliminary epicenters for January 1977 to March 1978: California Institute of Technology, Division of Geological and Planetary Sciences.

Whitcomb, J. H., Allen, C. R., Garmany, J. D., and Hileman, J. A., 1973, San Fernando earthquake series, 1971: focal mechanisms and tectonics: Reviews of Geophysics and Space Physics, v. 11, p. 693–730.

Wyss, Max, and Brune, J. N., 1968, Seismic moment, stress, and source dimensions for earthquakes in the California-Nevada region, Journal of Geophysical Research, v. 73, no. 14, p. 4681–4694.

Zoback, M. D., Tsukahara, Hiroaki, and Hickman, Stephen, 1980, Stress measurements at depth in the vicinity of the San Andreas fault: implications for the magnitude of shear stress at depth: Journal of Geophysical Research, v. 85, no. 11, p. 6157–6173.

Recent Reverse Faulting in the Transverse Ranges, California

U.S. GEOLOGICAL SURVEY PROFESSIONAL PAPER 1339